The Journal of the Astronautical Sciences, Vol. 56, No. 1, January–March 2008, pp. 121–134

Adaptive Satellite Attitude Control in the Presence of Inertia and CMG Gimbal Friction Uncertainties[1]

W. MacKunis,[2] K. Dupree,[2] N. Fitz-Coy,[2] and W. E. Dixon[2]

Abstract

A nonlinear adaptive attitude controller is designed in this paper that compensates for dynamic uncertainties in the spacecraft inertia matrix and unknown dynamic and static friction effects in the control moment gyroscope (CMG) gimbals. Attitude control torques are generated by means of a four single gimbal CMG pyramid cluster. The challenges to develop the adaptive controller are that the control input is multiplied by uncertainties due to dynamic friction effects and is embedded in a discontinuous nonlinearity due to static friction effects. A uniformly ultimately bounded result is proven via Lyapunov analysis for the case in which both static and dynamic gimbal friction is included in the dynamic model, and an extension is provided that illustrates how asymptotic tracking is achieved when only dynamic friction is present in the CMG model.

Introduction

Through ventures such as NASA's New Millennium Program and DoD's Operational Responsive Space [1], the space industry is moving toward smaller satellites and the buses that support them. Some proposed uses of these small satellites (small-sats) include astrophysics research, surveillance, and autonomous servicing, all of which require precision attitude motion. However, due to their smaller sizes, the attitude motion of these small-sats is more susceptible to external disturbances than their larger counterparts. Furthermore, the smaller sizes of these new small-sats limit the mass, power and size budgets allocated to their attitude control systems (ACS). These contradictory requirements necessitate novel solutions for the ACS.

Controllers that are based on the assumption that a torque can be directly applied about the body-fixed satellite axes (e.g., [2]–[5]) may not be well-suited for applications that require high-precision attitude control, because the satellite torques are

[1]Presented as paper AIAA 2007-6432 at the 2007 AIAA Guidance, Navigation, and Control Conference in Hilton Head, South Carolina, August 20–23, 2007.
[2]Department of Mechanical and Aerospace Engineering, University of Florida, Gainesville, FL 32611-6250, USA. E-mail: {mackunis, kdupree, nfc, wdixon}@ufl.edu.

generated by actuators with additional dynamics. For example, (especially in small rigid-body satellites), the desired torques are typically generated by a cluster (e.g., [6], [7]) of single gimbal control moment gyroscopes (CMGs) due to their low mass and low power consumption properties. Unfortunately, the torque producing capacity of CMGs can deteriorate over time due to changes in the dynamics such as bearing degradation and increased friction in the gimbals. The ramifications of CMG friction buildup include increased power consumption due to energy dissipation. Examples of actual satellite failures resulting from CMG problems are the Hipparcos satellite and Magellan satellite [8]. Hipparcos failed and "spun down" due to numerous gyroscope failures. One of these failures was due to high and variable drag torque in gyro Number 4, which led to premature degradation. The Magellan satellite was in transit to Venus for five months before it began exhibiting erratic motor current shifts in one of its gyros [8]. The cause of this failure was found to be friction buildup due to a manufacturing process error in which the bearing lubricant was contaminated by a solvent.

Motivated by the aforementioned issues, the problem of satellite attitude control in the presence of uncertainties has been investigated by several researchers. In [9], an output feedback structured model reference adaptive controller is developed for spacecraft rendezvous and docking problems. The adaptive controller in [9] accommodates inertia uncertainty in the momentum wheel actuator dynamics; however, no frictional effects were assumed to be present in the actuator model. A quaternion-based, full-state feedback attitude tracking controller was designed in [2] for a rigid satellite in the presence of an unknown satellite inertia matrix. A model-error control synthesis (MECS) approach was used in [3] to cancel the effects of modelling errors and external disturbances on the system. The control law proposed in [3] requires a model-error term to cancel the effects of a time delay, which is inherent to the MECS design. An adaptive control law is designed in [10], which incorporates a velocity-generating filter from attitude measurements. The controller in [10] is shown to achieve asymptotic convergence of the attitude and angular velocity tracking errors despite uncertainty in the satellite inertia, but it assumes no dynamic uncertainty in the control torque. While the aforementioned controllers perform well for applications involving large satellites, they may not be well-suited for attitude control of CMG-actuated small-sats. In this paper, we develop a more suitable control design for such small-sats.

A nonlinear adaptive controller is developed in this paper that compensates for inertia uncertainties and uncertain CMG gimbal friction. Instead of developing a control torque to solve the attitude tracking problem, the attitude tracking controller in this paper is developed in terms of the CMG gimbal angular velocity. The development is complicated by the fact that the control input is multiplied by a time-varying, nonlinear uncertain matrix. Additional complications arise because the gimbal velocity control term is embedded inside of a discontinous nonlinearity (i.e., the standard signum function) resulting from the CMG static friction effects. A robust control method is used to mitigate the disturbance resulting from the static friction. In addition, potential singularities may exist in the Jacobian that transforms the torque produced by each CMG to desired torques about the satellite coordinate frame [11]. The singularity problem is circumvented by the use of a particular Jacobian pseudoinverse, coined the "singularity robust steering law," which was introduced in [12], and has been implemented in several aerospace vehicles (e.g., see [11] and [13]). A uniformly ultimately bounded (UUB) stability

result is proven via Lyapunov analysis for the case in which both static and dynamic friction effects are included in the CMG dynamic model. An asymptotic tracking extension is then formulated for the case where static friction effects are ignored.

Dynamic Model

The dynamic model for a rigid body CMG-actuated satellite can be expressed as [14], [15]

$$J\dot{\boldsymbol{\omega}} = -\boldsymbol{\omega}^{\times} J\boldsymbol{\omega} + \boldsymbol{\tau}_{cmg} - \dot{J}\boldsymbol{\omega} \tag{1}$$

In (1), $J(\boldsymbol{\delta}) \in \mathbb{R}^{3\times 3}$ represents the positive definite, symmetric satellite inertia matrix that is a function of the CMG gimbal angular position vector $\boldsymbol{\delta}(t) \in \mathbb{R}^4$, $\boldsymbol{\omega}(t) \in \mathbb{R}^3$ denotes the angular velocity of the satellite body-fixed frame $\mathcal{F}$ with respect to $\mathcal{I}$ expressed in $\mathcal{F}$, $\boldsymbol{\tau}_{cmg}(t) \in \mathbb{R}^3$ denotes the torque generated via a CMG cluster consisting of four single gimbal CMGs, the term $\dot{J}(t)\boldsymbol{\omega}(t)$ represents the time variation of the satellite inertia matrix due to the motion of the CMGs, and the notation $\boldsymbol{\zeta}^{\times}\ \forall \boldsymbol{\zeta} = [\zeta_1, \zeta_2, \zeta_3]^{\mathrm{T}}$ denotes the skew-symmetric matrix

$$\boldsymbol{\zeta}^{\times} = \begin{bmatrix} 0 & -\zeta_3 & \zeta_2 \\ \zeta_3 & 0 & -\zeta_1 \\ -\zeta_2 & \zeta_1 & 0 \end{bmatrix} \tag{2}$$

The satellite inertia matrix in (1) can be lower and upper bounded as

$$\frac{1}{2}\lambda_{\min}\{J\}\|\boldsymbol{\xi}\|^2 \leq \boldsymbol{\xi}^{\mathrm{T}} J\boldsymbol{\xi} \leq \frac{1}{2}\lambda_{\max}\{J\}\|\boldsymbol{\xi}\|^2 \qquad \forall \boldsymbol{\xi} \in \mathbb{R}^n \tag{3}$$

where $\lambda_{\min}\{J\}$, $\lambda_{\max}\{J\} \in \mathbb{R}$ are the minimum and maximum eigenvalues of $J(\boldsymbol{\delta})$, respectively. The torque generated from the CMG cluster can be modeled as

$$\boldsymbol{\tau}_{cmg} = -(\dot{\mathbf{h}}_{cmg} + \boldsymbol{\omega}^{\times}\mathbf{h}_{cmg}) - AF_d\,\dot{\boldsymbol{\delta}} - AF_s\ \mathrm{sgn}\,\dot{\boldsymbol{\delta}} \tag{4}$$

where F_d, $F_s \in \mathbb{R}^{4\times 4}$ are diagonal matrices whose elements are the unknown constant dynamic and static friction coefficients, respectively, of the four CMG gimbals. Also in (4), $\mathbf{h}_{cmg}(t) \in \mathbb{R}^3$ represents the angular momentum of the CMG cluster, and $\dot{\mathbf{h}}_{cmg}(t)$ is modeled as [7]

$$\dot{\mathbf{h}}_{cmg} = hA\dot{\boldsymbol{\delta}} \tag{5}$$

where $h \in \mathbb{R}$ represents the constant angular momentum of each CMG expressed in the gimbal-fixed frame (i.e., h is the same for all four CMGs). The CMG torque expression in (4) and (5) does not explicitly include gimbal acceleration terms, but under the standard assumption that these sources of error are small by comparison, these effects are assumed to be included with the other bounded uncertainties, which contribute to the ultimate bound on the tracking error. In (4) and (5), $\dot{\boldsymbol{\delta}}(t) \in \mathbb{R}^4$ denotes the CMG gimbal angular velocity control input, which is defined as

$$\dot{\boldsymbol{\delta}} \triangleq [\dot{\delta}_1 \quad \dot{\delta}_2 \quad \dot{\delta}_3 \quad \dot{\delta}_4]^{\mathrm{T}} \tag{6}$$

where $\dot{\delta}_i(t) \in \mathbb{R}$ denotes the angular velocity of the individual CMG gimbals $\forall i = 1, 2, 3, 4$, $\mathrm{sgn}(\dot{\boldsymbol{\delta}}(t)) \in \mathbb{R}^4$ denotes a vector form of the standard $\mathrm{sgn}(\cdot)$ function where the $\mathrm{sgn}(\cdot)$ is applied to each element of $\dot{\boldsymbol{\delta}}(t)$, and $A(\boldsymbol{\delta}) \in \mathbb{R}^{3\times 4}$ denotes a measurable Jacobian matrix defined as

$$A = \begin{bmatrix} -\cos\gamma\cos\delta_1 & \sin\delta_1 & \sin\gamma\cos\delta_1 \\ \sin\delta_2 & -\cos\gamma\cos\delta_2 & \sin\gamma\cos\delta_2 \\ \cos\gamma\cos\delta_3 & \sin\delta_3 & \sin\gamma\cos\delta_3 \\ -\sin\delta_4 & \cos\gamma\cos\delta_4 & \sin\gamma\cos\delta_4 \end{bmatrix}^{\mathrm{T}} \tag{7}$$

where $\gamma \in \mathbb{R}$ is the constant angle (54.74 deg) of each wall of the pyramid-shaped CMG cluster as depicted in Fig. 1. Since the elements of $A(\boldsymbol{\delta})$ in equation (7) are combinations of bounded trigonometric terms, an inequality can be developed as

$$\|A(\boldsymbol{\delta})\|_{i\infty} \leq \zeta_0 \tag{8}$$

where $\zeta_0 \in \mathbb{R}$ is a positive bounding constant, and $\|\cdot\|_{i\infty}$ denotes the induced infinity norm of a matrix.

Kinematic Model

The rotational kinematics of the rigid-body satellite can be determined as [2]

$$\dot{\mathbf{q}}_v = \frac{1}{2}(\mathbf{q}_v^{\times}\boldsymbol{\omega} + q_0\boldsymbol{\omega}) \tag{9}$$

$$\dot{q}_0 = -\frac{1}{2}\mathbf{q}_v^{\mathrm{T}}\boldsymbol{\omega} \tag{10}$$

In equations (9) and (10), $\mathbf{q}(t) \triangleq \{q_0(t), \mathbf{q}_v(t)\} \in \mathbb{R} \times \mathbb{R}^3$ represents the unit quaternion [14] describing the orientation of the body-fixed frame $\mathcal{F}$ with respect to $\mathcal{I}$, subject to the constraint

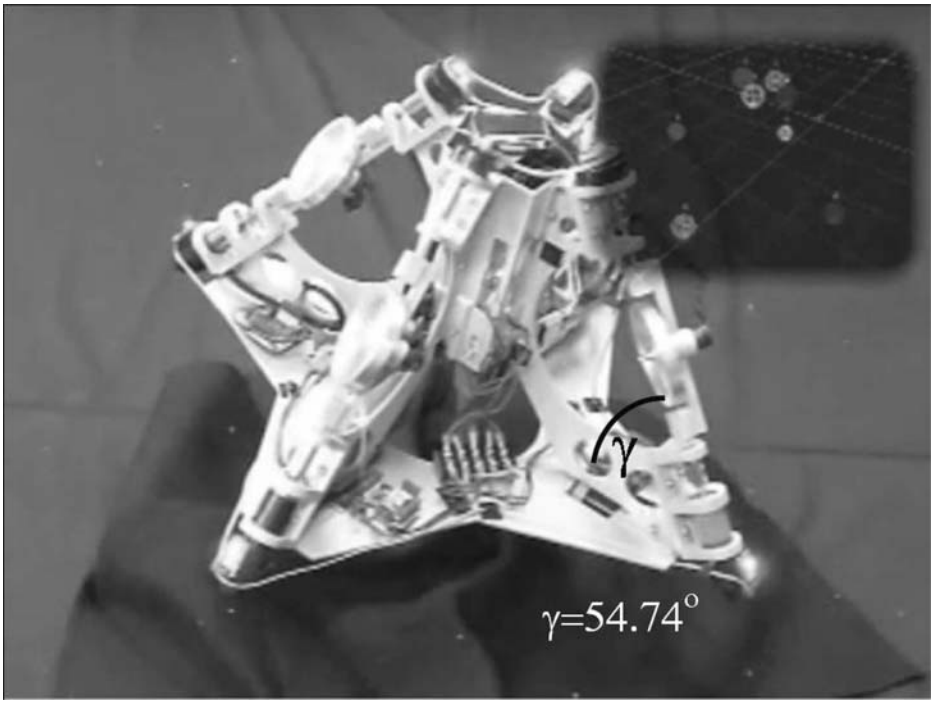

FIG. 1. The University of Florida Space Systems Group Control Moment Gyroscope Model.

$$\mathbf{q}_v^{\mathrm{T}}\mathbf{q}_v + q_0^2 = 1 \tag{11}$$

Rotation matrices that bring $\mathcal{I}$ onto $\mathcal{F}$ and $\mathcal{I}$ onto $\mathcal{F}_d$ (desired body-fixed orientation), denoted by $R(q_v, q_0) \in SO(3)$ and $R_d(q_{vd}, q_{0d}) \in SO(3)$, respectively, can be defined as

$$R \triangleq (q_0^2 - \mathbf{q}_v^{\mathrm{T}}\mathbf{q}_v)I_3 + 2\mathbf{q}_v\mathbf{q}_v^{\mathrm{T}} - 2q_0\mathbf{q}_v^{\times} \tag{12}$$

$$R_d \triangleq (q_{0d}^2 - \mathbf{q}_{vd}^{\mathrm{T}}\mathbf{q}_{vd})I_3 + 2\mathbf{q}_{vd}\mathbf{q}_{vd}^{\mathrm{T}} - 2q_{0d}\mathbf{q}_{vd}^{\times} \tag{13}$$

where I_3 denotes the 3×3 identity matrix, and $\mathbf{q}_d(t) \triangleq \{q_{0d}(t), \mathbf{q}_{vd}(t)\} \in \mathbb{R} \times \mathbb{R}^3$ represents the desired unit quaternion that describes the orientation of the body-fixed frame $\mathcal{F}_d$ with respect to $\mathcal{I}$. Using equations (9) and (10), $\boldsymbol{\omega}(t)$ can be expressed in terms of the quaternion as

$$\boldsymbol{\omega} = 2(q_0\dot{\mathbf{q}}_v - \mathbf{q}_v\dot{q}_0) - 2\mathbf{q}_v^{\times}\dot{\mathbf{q}}_v \tag{14}$$

The angular velocity of the desired body-fixed frame $\mathcal{F}_d$ with respect to $\mathcal{I}$ expressed in $\mathcal{F}_d$ can also be determined as

$$\boldsymbol{\omega}_d = 2(q_{0d}\dot{\mathbf{q}}_{vd} - \mathbf{q}_{vd}\dot{q}_{0d}) - 2\mathbf{q}_{vd}^{\times}\dot{\mathbf{q}}_{vd} \tag{15}$$

The subsequent analysis is based on the assumption that $q_{0d}(t)$, $\mathbf{q}_{vd}(t)$, and their first three time derivatives are bounded for all time. This assumption ensures that $\boldsymbol{\omega}_d(t)$ of (15) and its first two time derivatives are bounded for all time.

Control Objective

The objective in this paper is to develop a gimbal velocity controller to enable the attitude of $\mathcal{F}$ to track the attitude of $\mathcal{F}_d$. To quantify the objective, an attitude tracking error denoted by $\tilde{R}(\mathbf{e}_v, e_0) \in \mathbb{R}^{3\times3}$ is defined that brings $\mathcal{F}_d$ onto $\mathcal{F}$ as

$$\tilde{R} \triangleq RR_d^{\mathrm{T}} = (e_0^2 - \mathbf{e}_v^{\mathrm{T}}\mathbf{e}_v)I_3 + 2\mathbf{e}_v\mathbf{e}_v^{\mathrm{T}} - 2e_0\mathbf{e}_v^{\times} \tag{16}$$

where $R(\mathbf{q}_v, q_0)$ and $R_d(\mathbf{q}_{vd}, q_{0d})$ were defined in equations (12) and (13), respectively, and the quaternion tracking error $\mathbf{e}(t) \triangleq \{e_0(t), \mathbf{e}_v(t)\} \in \mathbb{R} \times \mathbb{R}^3$, is defined as

$$e_0 \triangleq q_0q_{0d} + \mathbf{q}_v^{\mathrm{T}}\mathbf{q}_{vd} \tag{17}$$

$$\mathbf{e}_v \triangleq q_{0d}\mathbf{q}_v - q_0\mathbf{q}_{vd} + \mathbf{q}_v^{\times}\mathbf{q}_{vd} \tag{18}$$

Based on equation (16), the attitude control objective can be stated as

$$\tilde{R}(\mathbf{e}_v(t), e_0(t)) \longrightarrow I_3 \qquad \text{as} \qquad t \longrightarrow \infty \tag{19}$$

Based on the tracking error formulation, the angular velocity of $\mathcal{F}$ with respect to $\mathcal{F}_d$ expressed in $\mathcal{F}$, denoted by $\tilde{\boldsymbol{\omega}}(t) \in \mathbb{R}^3$, is defined as

$$\tilde{\boldsymbol{\omega}} \triangleq \boldsymbol{\omega} - \tilde{R}\boldsymbol{\omega}_d \tag{20}$$

From the definitions of the quaternion tracking error variables, a constraint is developed as [2]

$$\mathbf{e}_v^{\mathrm{T}}\mathbf{e}_v + e_0^2 = 1 \tag{21}$$

where

$$0 \leq \|\mathbf{e}_v(t)\| \leq 1 \qquad 0 \leq |e_0(t)| \leq 1 \tag{22}$$

where $\|\cdot\|$ represents the standard Euclidean norm. From (21),

$$\|\mathbf{e}_v(t)\| \to 0 \Rightarrow |e_0(t)| \to 1 \tag{23}$$

and hence, equation (16) can be used to conclude that if equation (23) is satisfied, then the control objective in equation (19) will be achieved.

Adaptive Control Development

To facilitate the controller design, an auxiliary signal, denoted by $\mathbf{r}(t) \in \mathbb{R}^3$, is defined as

$$\mathbf{r} \triangleq \boldsymbol{\omega} - \tilde{R}\boldsymbol{\omega}_d + \alpha \mathbf{e}_v \tag{24}$$

where $\alpha \in \mathbb{R}^{3\times 3}$ is a constant, positive definite, diagonal control gain matrix. After substituting equation (24) into equation (20), the angular velocity tracking error can be expressed as

$$\tilde{\boldsymbol{\omega}} = \mathbf{r} - a\mathbf{e}_v \tag{25}$$

Motivation for the design of $\mathbf{r}(t)$ is obtained from the subsequent Lyapunov-based stability analysis and the fact that equations (14)–(18) can be used to determine the open-loop quaternion tracking error as

$$\dot{\mathbf{e}}_v = \frac{1}{2}(\mathbf{e}_v^{\times} + e_0 I)\tilde{\boldsymbol{\omega}} \qquad \dot{e}_0 = -\frac{1}{2}\mathbf{e}_v^{\mathrm{T}}\tilde{\boldsymbol{\omega}} \tag{26}$$

After taking the time derivative of equation (24) and premultiplying by $J(\boldsymbol{\delta})$, an expression can be obtained as

$$J\dot{\mathbf{r}} = J\dot{\boldsymbol{\omega}} + J\boldsymbol{\omega}^{\times}\tilde{R}\boldsymbol{\omega}_d - J\tilde{R}\dot{\boldsymbol{\omega}}_d + J\alpha\dot{\mathbf{e}}_v \tag{27}$$

where the fact that

$$\dot{\tilde{R}} = -\boldsymbol{\omega}^{\times}\tilde{R}$$

was utilized. After using equations (1), (4), (5), (24), and (26), the expression in equation (27) can be written as

$$J\dot{\mathbf{r}} = -\boldsymbol{\omega}^{\times}\mathbf{h}_{cmg} - \frac{1}{2}\dot{J}\mathbf{r} + Y_1\boldsymbol{\theta}_1 - \Omega_1\dot{\boldsymbol{\delta}} - hA\dot{\boldsymbol{\delta}} - AF_s \operatorname{sgn}\dot{\boldsymbol{\delta}} \tag{28}$$

In equation (28), $Y_1(\mathbf{e}_v, e_0, \boldsymbol{\omega}, \boldsymbol{\delta}, t) \in \mathbb{R}^{3\times p_1}$ is a known and measurable regression matrix, and $\boldsymbol{\theta}_1 \in \mathbb{R}^{p_1}$ is a vector of p_1 unknown constants where

$$Y_1\boldsymbol{\theta}_1 = -\boldsymbol{\omega}^{\times}J\boldsymbol{\omega} + J\boldsymbol{\omega}^{\times}\tilde{R}\boldsymbol{\omega}_d - J\tilde{R}\dot{\boldsymbol{\omega}}_d + \frac{1}{2}J\alpha(\mathbf{e}_v^{\times} + e_0 I)\tilde{\boldsymbol{\omega}} \tag{29}$$

The constant p_1 is defined based on the number of uncertain parameters in the parameterization in equation (29). In this case, $p_1 = 10$, corresponding to three uncertain gimbal inertia parameters, three uncertain satellite inertia parameters, and four uncertain CMG mass parameters. Also in equation (28), $\Omega_1(\mathbf{r}, \mathbf{e}_v, e_0, t) \in \mathbb{R}^{3\times 4}$ denotes an auxiliary matrix containing parametric uncertainty defined as

$$\Omega_1\dot{\boldsymbol{\delta}} = \left(\frac{\partial J}{\partial \delta}\dot{\boldsymbol{\delta}}\right)\left(\frac{1}{2}\mathbf{r} + \tilde{R}\boldsymbol{\omega}_d + \alpha\mathbf{e}_v\right) + AF_d\dot{\boldsymbol{\delta}} \tag{30}$$

that can be linearly parameterized in terms of a known regression matrix $Y_2(\mathbf{e}_v, e_0, \mathbf{r}, \boldsymbol{\omega}, \boldsymbol{\delta}, \dot{\boldsymbol{\delta}}, t) \in \mathbb{R}^{3\times p2}$ and a vector of p_2 unknown constants $\boldsymbol{\theta}_2 \in \mathbb{R}^{p2}$ as

$$\Omega_1 \dot{\boldsymbol{\delta}} \triangleq Y_2 \boldsymbol{\theta}_2 \tag{31}$$

The constant p_2 is defined based on the number of uncertain elements in equation (30). In this case, $p_2 = 6$, corresponding to two uncertain CMG inertia parameters and four uncertain dynamic friction coefficients. Some of the control design challenges for the open-loop system in equation (28) are that the control input $\dot{\boldsymbol{\delta}}(t)$ is premultiplied by a nonsquare known time-varying matrix plus a nonsquare unknown time-varying matrix, and $\dot{\boldsymbol{\delta}}(t)$ is embedded inside of a discontinuous nonlinearity (i.e., the *signum* function). To address the fact that $\dot{\boldsymbol{\delta}}(t)$ is premultiplied by a nonsquare unknown time-varying matrix, an estimate of the uncertainty in equation (31), denoted by $\hat{\Omega}_1(\mathbf{r}, \mathbf{e}_v, e_0, t) \in \mathbb{R}^{3\times 4}$, is defined as

$$\hat{\Omega}_1 \dot{\boldsymbol{\delta}} \triangleq Y_2 \hat{\boldsymbol{\theta}}_2 \tag{32}$$

where $\hat{\boldsymbol{\theta}}_2(t) \in \mathbb{R}^{p2}$ is a subsequently designed estimate for the parametric uncertainty in $\Omega_1(\mathbf{r}, \mathbf{e}_v, e_0, t)$. Based on equations (31) and (32), equation (28) can be rewritten as

$$J\dot{\mathbf{r}} = -\boldsymbol{\omega}^{\times}\mathbf{h}_{cmg} - \frac{1}{2}\dot{J}\mathbf{r} + Y_1\boldsymbol{\theta}_1 - Y_2\tilde{\boldsymbol{\theta}}_2 - B\dot{\boldsymbol{\delta}} - AF_s \operatorname{sgn}\dot{\boldsymbol{\delta}} \tag{33}$$

where $B(\mathbf{r}, \mathbf{e}_v, e_0, \boldsymbol{\delta}, t) \in \mathbb{R}^{3\times 4}$ is defined as

$$B = hA + \hat{\Omega}_1 \tag{34}$$

and the parameter estimate mismatch $\tilde{\boldsymbol{\theta}}_2(t) \in \mathbb{R}^{p2}$ is defined as

$$\tilde{\boldsymbol{\theta}}_2 = \boldsymbol{\theta}_2 - \hat{\boldsymbol{\theta}}_2 \tag{35}$$

Based on the expression in equation (33) and the subsequent stability analysis, the control input is designed as

$$\dot{\boldsymbol{\delta}} = B^{+}[Y_1\hat{\boldsymbol{\theta}}_1 - \boldsymbol{\omega}^{\times}\mathbf{h}_{cmg} + k\mathbf{r} + k_n\mathbf{r} + \mathbf{e}_v] \tag{36}$$

where $k, k_n \in \mathbb{R}$ denote positive control gains, and $B^{+}(\mathbf{r}, \mathbf{e}_v, e_0, \boldsymbol{\delta}, t) \in \mathbb{R}^{4\times 3}$ denotes a pseudoinverse of $B(\boldsymbol{\delta}, \mathbf{e}_v, e_0, \hat{\boldsymbol{\theta}}_2, t)$ defined as [11]–[13]

$$B^{+} = B^{\mathrm{T}}(BB^{\mathrm{T}} + \epsilon I_{3\times 3})^{-1} \tag{37}$$

In equation (37), $\epsilon(t) \in \mathbb{R}$ denotes a singularity avoidance parameter. For example, Nakamura et al. [12] designed $\epsilon(t)$ as

$$\epsilon \triangleq \epsilon_0 \exp[-\det(BB^{\mathrm{T}})] \tag{38}$$

so that $\epsilon(t)$ is negligible when $B(\mathbf{r}, \mathbf{e}_v, e_0, \boldsymbol{\delta}, t)\, B^{\mathrm{T}}(\mathbf{r}, \mathbf{e}_v, e_0, \boldsymbol{\delta}, t)$ is nonsingular but increases to the constant parameter $\epsilon_0 \in \mathbb{R}$ as the singularity is approached. After substituting the control input expression in equation (36) into equation (33), an expression is obtained as

$$J\dot{\mathbf{r}} = -\frac{1}{2}\dot{J}\mathbf{r} + Y_1\tilde{\boldsymbol{\theta}}_1 - Y_2\tilde{\boldsymbol{\theta}}_2 - k\mathbf{r} - k_n\mathbf{r} - \mathbf{e}_v - AF_s \operatorname{sgn}\dot{\boldsymbol{\delta}} \tag{39}$$

where the parameter estimate mismatch $\tilde{\boldsymbol{\theta}}_1(t) \in \mathbb{R}^{p1}$ is defined as

$$\tilde{\boldsymbol{\theta}}_1 = \boldsymbol{\theta}_1 - \hat{\boldsymbol{\theta}}_1 \tag{40}$$

Based on equation (39) and the subsequent stability analysis, the parameter estimates $\hat{\boldsymbol{\theta}}_1(t)$ and $\hat{\boldsymbol{\theta}}_2(t)$ are designed as

$$\dot{\hat{\boldsymbol{\theta}}}_1 = \text{proj}(\Gamma_1 Y_1^{\mathrm{T}}\mathbf{r}) \qquad \dot{\hat{\boldsymbol{\theta}}}_2 = \text{proj}(-\Gamma_2 Y_2^{\mathrm{T}}\mathbf{r}) \tag{41}$$

where $\Gamma_1 \in \mathbb{R}^{p1\times p1}$ and $\Gamma_2 \in \mathbb{R}^{p2\times p2}$ denote constant, positive-definite, diagonal adaptation gain matrices, and $\text{proj}(\cdot)$ denotes a projection algorithm utilized to guarantee that the ith element of $\hat{\boldsymbol{\theta}}_1(t)$ and $\hat{\boldsymbol{\theta}}_2(t)$ can be bounded as

$$\underline{\theta}_{1i} \le \hat{\theta}_{1i} \le \bar{\theta}_{1i} \qquad \underline{\theta}_{2i} \le \hat{\theta}_{2i} \le \bar{\theta}_{2i} \tag{42}$$

where $\underline{\theta}_{1i}$, $\bar{\theta}_{1i} \in \mathbb{R}$ and $\underline{\theta}_{2i}$, $\bar{\theta}_{2i} \in \mathbb{R}$ denote known, constant lower and upper bounds for each element of $\hat{\boldsymbol{\theta}}_1(t)$ an $\hat{\boldsymbol{\theta}}_2(t)$, respectively.

Remark 1: While robust or linear control methods (i.e., LQR, H_∞, LQG) can be applied to linearized versions of satellite systems, such controllers are designed based on worst-case scenarios for the uncertainty in the system. Although high gain and/or high frequency feedback can be used to compensate for such worst-case scenarios, adaptive control has advantages over linear or robust control approaches in that high gain and/or high frequency feedback is not necessary.

Stability Analysis

Theorem 1: Given the closed-loop error dynamics in equation (39), the adaptive controller of equation (36) and equation (41) ensures global uniformly ultimately bounded (GUUB) attitude tracking in the sense that

$$\|\mathbf{e}_v(t)\| \to \epsilon_0 \exp(-\epsilon_1 t) + \epsilon_2 \tag{43}$$

where ϵ_0, ϵ_1, $\epsilon_2 \in \mathbb{R}$ denote positive bounding constants.

Let $V(e_0, \mathbf{e}_v, \mathbf{r}, t) \in \mathbb{R}$ be defined as the nonnegative function

$$V \triangleq \mathbf{e}_v^{\mathrm{T}}\mathbf{e}_v + (1 - e_0)^2 + \frac{1}{2}\mathbf{r}^{\mathrm{T}}J\mathbf{r} + \frac{1}{2}\tilde{\boldsymbol{\theta}}_1^{\mathrm{T}}\Gamma_1^{-1}\tilde{\boldsymbol{\theta}}_1 + \frac{1}{2}\tilde{\boldsymbol{\theta}}_2^{\mathrm{T}}\Gamma_2^{-1}\tilde{\boldsymbol{\theta}}_2 \tag{44}$$

It follows directly from the bounds given in equations (3), (22), and (42) that $V(e_0, \mathbf{e}_v, \mathbf{r}, t)$ can be upper and lower bound as

$$\lambda_1\|\mathbf{z}\|^2 + c_1 \le V(t) \le \lambda_2\|\mathbf{z}\|^2 + c_2 \tag{45}$$

where λ_1, λ_2, c_1, $c_2 \in \mathbb{R}$ are known positive bounding constants, and $\mathbf{z}(t) \in \mathbb{R}^6$ is defined as

$$\mathbf{z} \triangleq [e_v^{\mathrm{T}} \quad r^{\mathrm{T}}]^{\mathrm{T}} \tag{46}$$

After using equations (26), (35), (39), and (40), the time derivative of $V(e_0, \mathbf{e}_v, \mathbf{r}, t)$ can be expressed as

$$\begin{aligned}\dot{V} = {} & e_v^{\mathrm{T}}(\mathbf{e}_v^{\times} + e_0 I)\tilde{\boldsymbol{\omega}} + (1 - e_0)e_v^{\mathrm{T}}\tilde{\boldsymbol{\omega}} \\ & + \mathbf{r}^{\mathrm{T}}(Y_1\tilde{\boldsymbol{\theta}}_1 - Y_2\tilde{\boldsymbol{\theta}}_2 - k\mathbf{r} - k_n\mathbf{r} - \mathbf{e}_v - AF_s \operatorname{sgn}\dot{\boldsymbol{\delta}}) \\ & - \tilde{\boldsymbol{\theta}}_1^{\mathrm{T}}\Gamma_1^{-1}\dot{\hat{\boldsymbol{\theta}}}_1 - \tilde{\boldsymbol{\theta}}_2^{\mathrm{T}}\Gamma_2^{-1}\hat{\boldsymbol{\theta}}_2\end{aligned} \tag{47}$$

By using equations (8), (25), (41), and exploiting the fact that

$$\mathbf{e}_v^{\mathrm{T}}\mathbf{e}_v^{\times}\tilde{\boldsymbol{\omega}} = 0$$

the expression in equation (47) can be written as

$$\dot{V} \leq -\lambda_3 \|\mathbf{z}\|^2 - k_n \|\mathbf{r}\|^2 + \|\mathbf{r}\| \zeta_0 \|F_s\|_{i\infty} \tag{48}$$

where $\lambda_3 = \lambda_{\min}\{a, k\} \in \mathbb{R}$. After completing the squares, equation (48) can be written as

$$\dot{V}(t) \leq -\lambda_3 \|\mathbf{z}\|^2 + \frac{(\zeta_0 \|F_s\|_{i\infty})^2}{4k_n} \tag{49}$$

Since the inequality in equation (45) can be utilized to lower bound $\|\mathbf{z}\|^2$ as

$$\|\mathbf{z}\|^2 \geq \frac{1}{\lambda_2} V(t) - \frac{c_2}{\lambda_2} \tag{50}$$

the inequality in equation (49) can be expressed as

$$\dot{V}(t) \leq -\frac{\lambda_3}{\lambda_2} V(t) + \boldsymbol{\epsilon} \tag{51}$$

where $\boldsymbol{\epsilon} \in \mathbb{R}$ is a positive constant that is defined as

$$\boldsymbol{\epsilon} = \frac{(\zeta_0 \|F_s\|_{i\infty})^2}{4k_n} + \frac{\lambda_3 c_2}{\lambda_2} \tag{52}$$

The linear differential inequality in equation (51) can be solved as

$$V(t) \leq V(0) \exp\left(-\frac{\lambda_3}{\lambda_2}\right) t + \boldsymbol{\epsilon} \frac{\lambda_2}{\lambda_3} \left[1 - \exp\left(-\frac{\lambda_3}{\lambda_2} t\right)\right] \tag{53}$$

The expressions in equations (44) and (53) can be used to conclude that $\mathbf{r}(t) \in \mathcal{L}_\infty$. Thus, from equations (22), (25), and (46), $\tilde{\boldsymbol{\omega}}(t)$, $\mathbf{z}(t) \in \mathcal{L}_\infty$, and equation (24) can be used to conclude that $\boldsymbol{\omega}(t) \in \mathcal{L}_\infty$. Equation (26) then shows that $\dot{\mathbf{e}}_v(t)$, $\dot{e}_0(t) \in \mathcal{L}_\infty$. Hence, equations (29), (32), (34), and (42) can be used to prove that the control input $\dot{\boldsymbol{\delta}}(t) \in \mathcal{L}_\infty$. Standard signal chasing arguments can then be utilized to prove that all remaining signals remain bounded during closed-loop operation. The inequalities in equation (45) can now be used along with equations (52) and (53) to conclude that

$$\|\mathbf{z}\|^2 \leq \left(\frac{\lambda_2 \|z(0)\|^2 + c_2}{\lambda_1}\right) \exp\left\{-\frac{\lambda_3}{\lambda_2} t\right\} + \left(\frac{\lambda_2 (\zeta_0 \|F_s\|_{i\infty})^2}{4k_n \lambda_3 \lambda_1} + \frac{c_2 - c_1}{\lambda_1}\right) \tag{54}$$

The result in equation (43) can now be directly obtained from equation (54).

Asymptotic Tracking Extension

In this section, a control design is developed for the case when static friction F_s is ignored. The following analysis illustrates that the controller developed in the previous section can be used to achieve asymptotic attitude tracking for this case.

Closed-Loop Error System

In the absence of static friction, letting $k_n = 0$ in equation (36) results in an expression for the closed-loop tracking error system as

$$J\dot{\mathbf{r}} = -\frac{1}{2} \dot{J}\mathbf{r} + Y_1 \tilde{\boldsymbol{\theta}}_1 - Y_2 \tilde{\boldsymbol{\theta}}_2 - k\mathbf{r} + \mathbf{e}_v \tag{55}$$

Stability Analysis Ignoring Static Friction

Theorem 2: Given the closed-loop dynamics given in equation (55), the adaptive controller of equations (36) and (41) ensures asymptotic attitude tracking in the sense that

$$\|\mathbf{e}_v(t)\| \to 0 \qquad \text{and} \qquad \|\tilde{\boldsymbol{\omega}}(t)\| \to 0 \tag{56}$$

provided the initial conditions are selected such that

$$\|e_0(0)\| \neq 0 \tag{57}$$

and the inertia matrix J satisfies the sufficient condition defined in equation (3).

To prove Theorem 2, the same procedure as in the previous section can be used to calculate the time derivative of the function $V(t)$ defined in equation (44) as

$$\dot{V}(t) \leq -\lambda_3 \|\mathbf{z}\|^2 \tag{58}$$

where $\mathbf{z}$ was defined in equation (46), and λ_3 was defined in equation (48). From equation (58), $\dot{V}(t)$ is negative semi-definite, and $V(t)$ is bounded as shown in equation (45). Furthermore, equations (22), (24), (41), (42), and (55) can be used to conclude that $\mathbf{e}(t)$, $\dot{\mathbf{e}}(t)$, $\dot{\mathbf{r}}(t) \in \mathcal{L}_\infty$. Thus, $\dot{\mathbf{z}}(t) \in \mathcal{L}_\infty$, and $\mathbf{z}(t) \in \mathcal{L}_2 \cap \mathcal{L}_\infty$. Barbalat's Lemma can now be used to conclude that

$$\|\mathbf{z}(t)\| \to 0 \qquad \text{as} \qquad t \to \infty$$

Hence, the adaptive control law given by equations (36) and (41) achieves the asymptotic tracking claim given in equation (56) for the case in which static friction is ignored in the dynamics. Verification of the boundedness of the remaining signals during closed-loop operation is similar to that in the previous section.

Simulation Results

The attitude controller developed in this paper was simulated based on the model for the University of Florida CMG (see Fig. 1). Using equation (1), the dynamic equation of motion in terms of the CMG model can be expressed as

$$J_{cmg}\dot{\boldsymbol{\omega}} = -\boldsymbol{\omega}^{\times} J_{cmg}\boldsymbol{\omega} - \dot{J}_{cmg}\boldsymbol{\omega} - (\dot{\mathbf{h}}_{cmg} + \boldsymbol{\omega}^{\times}\mathbf{h}_{cmg}) - AF_d\dot{\boldsymbol{\delta}} - AF_s \operatorname{sgn}\dot{\boldsymbol{\delta}} \tag{59}$$

where the CMG inertia matrix $J_{cmg}(\boldsymbol{\delta}) \in \mathbb{R}^{3\times 3}$ is defined using the parallel axis theorem as

$$J_{cmg} \triangleq J_0 + \sum_{i=1}^{4} [{}^{B}J_{gi} + m_{cmgi}(\mathbf{r}_i^{\mathrm{T}}\mathbf{r}_i I_3 - \mathbf{r}_i\mathbf{r}_i^{\mathrm{T}})] \tag{60}$$

In equation (60), the CMG parameters $J_0 \triangleq J_{cmg}(0) = \operatorname{diag}\{0.0610 \quad 0.0610 \quad 0.0764\}\,\mathrm{kg\,m^2}$, $m_{cmgi} = 0.1565$ kg, $\mathbf{r}_i \in \mathbb{R}^3$ $\forall i = 1, 2, 3, 4$ are defined as[3]

$$\mathbf{r}_1 \triangleq [0.1591 \quad 0 \quad 0.1000]^{\mathrm{T}}\mathrm{m} \tag{61}$$

$$\mathbf{r}_2 \triangleq [-0.1591 \quad 0 \quad 0.1000]^{\mathrm{T}}\mathrm{m} \tag{62}$$

[3]The actual values for the parameters J_0, F_d, F_s, m_{cmgi}, and ${}^{gi}J_{gi}$ $\forall i = 1, 2, 3, 4$ are used to generate the plant model in the simulation, but they are not used in the control law. The adaptive control law compensates for these uncertain parameters.

$$\mathbf{r}_3 \triangleq [0 \quad 0.1591 \quad 0.1000]^{\mathrm{T}}\mathrm{m} \tag{63}$$

$$\mathbf{r}_4 \triangleq [0 \quad -0.1591 \quad 0.1000]^{\mathrm{T}}\mathrm{m} \tag{64}$$

${}^{B}J_{gi}(\boldsymbol{\delta}) \in \mathbb{R}^{3\times 3}\ \forall i = 1, 2, 3, 4$ denotes the inertia matrix of the ith gimbal as expressed in the CMG body-fixed frame defined as

$${}^{B}J_{gi} \triangleq [C_{Bgi}][{}^{gi}J_{gi}][C_{Bgi}]^{\mathrm{T}} \tag{65}$$

$\dot{\mathbf{h}}_{cmg} \in \mathbb{R}^3$ is defined using equation (5), where $h = 0.078$, and I_n denotes the $n \times n$ identity matrix. In equation (65), the coordinate transformation matrix $C_{Bgi} \in SO(3)\ \forall i = 1, 2, 3, 4$ relates the ith gimbal-fixed frame to the CMG body-fixed frame, and ${}^{gi}J_{gi} = \mathrm{diag}\{4.89 \times 10^{-5} \quad 2.49 \times 10^{-4} \quad 2.79 \times 10^{-4}\}\mathrm{kg\,m^2}$ $\forall i = 1, 2, 3, 4$ represents the inertia matrix of the ith gimbal as expressed in the ith gimbal-fixed frame.

The objective is to regulate a satellite's attitude to the desired quaternion defined by

$$\mathbf{q}_d = [0.808 \quad -0.174 \quad 0.556 \quad -0.091]^{\mathrm{T}} \tag{66}$$

with the initial quaternion orientation of the satellite given by

$$\mathbf{q}(0) = [1 \quad 0 \quad 0 \quad 0]^{\mathrm{T}}$$

and the adaptive estimates initialized as

$$\hat{\boldsymbol{\theta}}_1(0) = [0 \quad 0 \quad 0 \quad 0 \quad 0 \quad 0 \quad 0 \quad 0 \quad 0 \quad 0]^{\mathrm{T}}$$

$$\hat{\boldsymbol{\theta}}_2(0) = [0 \quad 0 \quad 0 \quad 0 \quad 0 \quad 0]^{\mathrm{T}}$$

Remark 2: In a realistic scenario, the adaptive estimates would be initialized to the best guess of the actual parameter values. The estimates were initialized to a vector of zeros in the simulation to test a case when no knowledge of the parameters is available. The simulation was also run using initial parameter estimates of ten times their actual value, with no noticeable degradation in controller performance.

The friction matrices F_d and F_s for the simulated CMG are (e.g., see reference [16])

$$F_d = 0.2I_4 \qquad F_s = 0.4I_4 \tag{67}$$

To test the scenario when a sudden increase in the friction occurs, an instantaneous jump (i.e., step function) of 0.3 in the F_d and F_s parameters is programmed to occur four seconds into the simulation.[4] To test a realistic scenario, random number noise of 10% was added to all sensor measurements in the simulation. In addition, an input delay of 10 ms was included to simulate the effects of gimbal servo loop delays. Figures 2–3 show the simulation results of the closed-loop system for this case with control gains selected as (e.g., see equations (36), (37), (38), and (41))

$$k = 0.5 \qquad k_n = 0.3 \qquad \boldsymbol{\epsilon}_0 = 0.2 \qquad \alpha = 0.2$$

$$\Gamma_1 = 0.025I_{10} \qquad \Gamma_2 = 1.1I_6$$

The steady-state quaternion tracking error is on the order of 10^{-3}. Figure 4 illustrates the variation in the inertia parameters during closed-loop operation.

[4]In a realistic situation, the gimbal friction would most likely increase gradually over time (e.g., due to bearing degradation, corrosion, etc.), so the sudden spike of friction tested in the simulation tests a worst-case scenario.

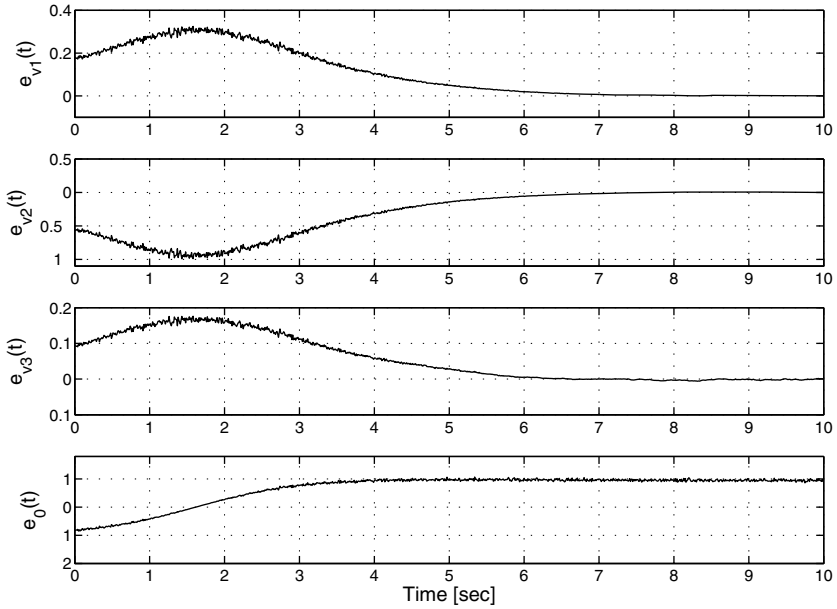

FIG. 2. Quaternion Tracking Error (no units).

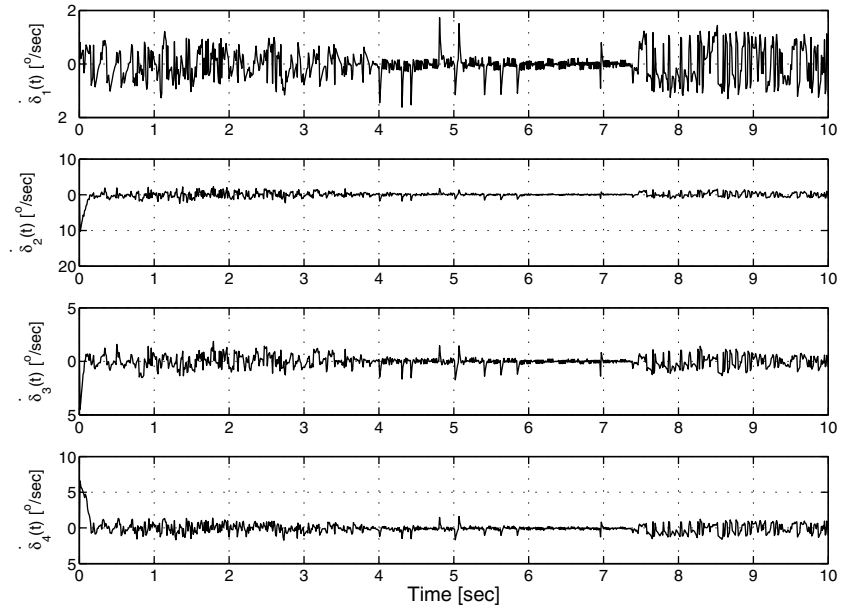

FIG. 3. Control Input Gimbal Angular Rates.

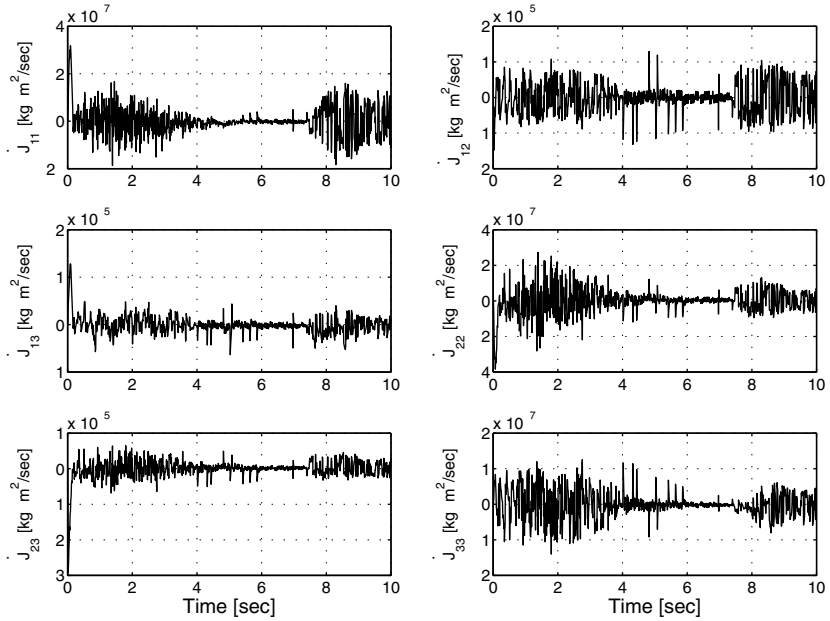

FIG. 4. $\dot{J}(\boldsymbol{\delta})$ vs. Time.

Conclusions and Future Work

In this paper, a uniformly ultimately bounded attitude tracking controller for a rigid-body satellite is presented. The controller adapts for parametric uncertainty in the satellite inertia matrix in addition to the uncertainties in the input torque caused by unknown CMG gimbal friction. The gimbal rate input controller achieves uniformly ultimately bounded attitude tracking in the presence of static and dynamic CMG gimbal friction. In the presence of static friction, the control design is complicated due to the control input being embedded in a discontinuous nonlinearity. This difficulty is overcome with the use of a robust tracking control law. In addition, since a singularity robust steering law was incorporated in the control design, the proposed approach avoids singular torque directions inherent to the dynamics of the four single gimbal CMG cluster. Numerical simulation results were provided to show the efficacy of the proposed controller. An asymptotic tracking extension is also presented in the absence of static friction in the dynamic model. Future work will address the issues of explicit gimbal acceleration dependence in the CMG torque model, variations in CMG wheel speed, and hard stops in the CMG gimbals.

Acknowledgments

This research is supported in part by the NSF CAREER award number 0547448, AFOSR contract number F49620-03-1-0170, by research grant No. US-3715-05 from BARD, the United States–Israel Binational Agricultural Research and Development Fund, and the Department of Energy, grant number DE-FG04-86NE37967 as part of the DOE University Research Program in Robotics (URPR).

References

[1] CEBROWSKI, A. and RAYMOND, J. "Operationally Responsive Space: A New Defense Business Model," *Parameters*, Vol. 35, No. 2, pp. 67–77, 2005.

[2] COSTIC, B., DAWSON, D., QUEIROZ, M. DE., and KAPILA, V. "A Quaternion-Based Adaptive Attitude Tracking Controller Without Velocity Measurements," *Proceedings of the IEEE Conference on Decision and Control*, Vol. 3, Sydney, Australia, December 2000, pp. 2424–2429.

[3] KIM, J. and CRASSIDIS, J. "Robust Spacecraft Attitude Control Using Model-Error Control Synthesis," *Proceedings of the AIAA Guidance, Navigation, and Control Conference*, Monterey, CA, August 2002.

[4] PAN, H., WONG, H., and KAPILA, V. "Output Feedback Control for Spacecraft with Coupled Translation and Attitude Dynamics," *Proceedings of IEEE Conference on Decision and Control*, Paradise Island, Bahamas, Dec. 2004, pp. 4453–4458.

[5] SUBBARAO, K. and AKELLA, M. R. "Differentiator-Free Nonlinear Proportional-Integral Controllers for Rigid-Body Attitude Stabilization," *Proceedings of the AAS/AIAA 14th Space Flight Mechanics Meeting*, Vol. 27, No. 6, 2004, pp. 1092–1096.

[6] LAPPAS, V., STEYN, W., and UNDERWOOD, C. "Design and Testing of a Control Moment Gyroscope Cluster for Small Satellites," *Journal of Spacecraft and Rockets*, Vol. 42, No. 4, 2005, pp. 729–739.

[7] OMAGARI, K., USUDA, T., and MATUNAGA, S. "Research of Control Momentum Gyros for Micro-Satellites and 3-DOF Attitude Dynamics Simulator Experiments," *Proceedings of the International Symposium on Artificial Intelligence, Robotics and Automation in Space*, Munich, Germany, 2005.

[8] HARLAND, D. M. and LORENZ, R. D. *Space Systems Failures*, J. Mason, Ed., Springer-Praxis, 2005.

[9] SINGLA, P., SUBBARAO, K., and JUNKINS, J. L. "Adaptive Output Feedback Control for Spacecraft Rendezvous and Docking Under Measurement Uncertainty," *Journal of Guidance, Control, and Dynamics*, Vol. 29, No. 4, 2006, pp. 892–902.

[10] WONG, H., QUEIROZ, M. DE., and KAPILA, V. "Adaptive Tracking Control Using Synthesized Velocity from Attitude Measurements," *Proceedings of the American Control Conference*, Vol. 3, 2000, pp. 1572–1576.

[11] FORD, K. A. and HALL, C. D. "Singular Direction Avoidance Steering for Control-Moment Gyros," *Journal of Guidance, Control, and Dynamics*, Vol. 23, No. 4, 2000, pp. 648–656.

[12] NAKAMURA, Y. and HANAFUSA, H. "Inverse Kinematic Solutions with Singularity Robustness for Robot Manipulator Control," *Journal of Dynamic Systems, Measurement, and Control*, Vol. 108, No. 3, 1986, pp. 163–171.

[13] BEDROSSIAN, N., PARADISO, J., BERGMANN, E., and ROWELL, D. "Steering Law Designs for Redundant SGCMG Systems," *Journal of Guidance, Control, and Dynamics*, Vol. 13, No. 6, 1991, pp. 1083–1089.

[14] HUGHES, P. *Spacecraft Attitude Dynamics*, Wiley, New York, 1994.

[15] KANE, T., LIKINS, P., and LEVINSON, D. *Spacecraft Dynamics*, McGraw-Hill, New York, 1983.

[16] LEVE, F., TATSCH, A., and FITZ-COY, N. "A Scalable Control Moment Gyro Design for Attitude Control of Micro-, Nano-, and Pico-Class Satellites," *Proceedings of the AAS Guidance and Control Conference*, Breckenridge, CO, 2007.